Chemical Science

Accepted Manuscript

This article can be cited before page numbers have been issued, to do this please use: W. Xie and M. Koyama, *Chem. Sci.*, 2019, DOI: 10.1039/C9SC00912D.

ROYAL SOCIETY OF CHEMISTRY

rsc.li/chemical-science

View Article Online
DOI: 10.1039/C9SC00912D

Theoretical design for a Technetium-like Alloy and its catalytic Properties.

Wei Xie[a, *], Michihisa Koyama[a, b ,c, *]

[*] Corresponding authors

[a] INAMORI Frontier Research Center, Kyushu University, 744 Motooka, Nishi-ku, Fukuoka, 819-0395, Japan

E-mail: xiewei@ifrc.kyushu-u.ac.jp

[b] Graduate School of Engineering, Hiroshima University, 1-4-1 Kagamiyama, Higashi-Hiroshima, Hiroshima 739-8527, Japan

View Article Online
DOI: 10.1039/C9SC00912D

[c] Global Research Center for Environment and Energy based on Nanomaterials Science, National Institute for Materials Science, 1-1 Namiki, Tsukuba, Ibaraki 305-0044, Japan

E-mail: koyama.michihisa@nims.go.jp

Abstract: Based on the concept of density of states (DOS) engineering, we theoretically designed a pseudo-Tc material (Mo–Ru alloy) and investigated its electronic structure, phase stability and catalytic activity by using density functional theory. Through comparing the DOS shape, peak distribution, and DOS area differences between Tc and the Mo–Ru alloy, we noticed that bcc-Mo_8Ru_8 and hcp-Mo_8Ru_8 had the most similar electronic structures to Tc. The excess energies after entropy correction of hcp-Mo_8Ru_8 and bcc-Mo_8Ru_8 are stable when the temperature is up to 765 and 745 K, respectively. These results provided the possibility of pseudo-Tc alloys (hcp-Mo_8Ru_8 and bcc-Mo_8Ru_8) synthesis. Finally, according to the reaction coordinate analysis, the similar

View Article Online
DOI: 10.1039/C9SC00912D

catalytic activity between the hcp-Mo_8Ru_8 and Tc have been proved in CO oxidation and N_2 dissociation. In N_2 dissociation, Tc have a suitable ratio of transition states (TS) barrier and reaction energy which make Tc be an efficient catalyst for NH_3 syntheses, as well as our designed pseudo-Tc (hcp-MoRu) because of similar electronic structures. Our finding provides valuable insight into materials and catalyst design.

KEYWORDS Electronic structures, pseudo-Tc alloy, Phase stability, Density functional theory

1 Introduction

Technetium (Tc) is the lightest element among the elements for which all isotopes are radioactive. It is unstable and extremely scarce, and only minute amounts are found in the earth's crust. Technetium was discovered in 1937 by Carlo Perrier and Emilio Segrè[1] and is named according to the Greek word for “artificial,” representing the fact that Tc is an element that is artificially made during nuclear reactions. Every year, a large amount of Tc is produced in nuclear waste. Except for the small portion used for

View Article Online
DOI: 10.1039/C9SC00912D

medical application, the disposition of Tc in nuclear waste is being taken into serious consideration. Of greatest concern is its relatively high mobility in aqueous and geochemical environments[2]. For the safe storage, the chemical properties of Tc have been investigated[3]. However, running chemical test experiments entails considerable risk. In recent decades, a few Tc studies have been conducted, including the effect of corrosion from Tc on Fe[4,5] and Zr[6] in steel containers and on the surface effect of Tc and its alloys in water and in an ambient environment[3,4]. Technetium is more effective as a dehydrogenation catalyst than rhenium and palladium[7], but its radioactivity limits its study and wide application.

Practically, Tc is too dangerous to use as a commodity or for industry applications. Nonetheless, its unexplored electronic structure may lead to unique functionality for certain applications. Recently, a new concept of density of states (DOS) engineering[8] has been proposed as a novel approach to engineer alloys' chemical properties. DOS engineering can be used for electronic structure design for a specific application. The chemical and physical properties of elements are determined by their electronic states, which can be expressed as DOS[9–12]. Based on tuning the location of the d-band center

View Article Online
DOI: 10.1039/C9SC00912D

from DOS results, d-band theory has been used for catalytic design[11,12]. According to the intended chemical and physical properties, the suitable DOS shape also is a key matter. By alloying every available element, we may be able to manipulate the shape of the DOS as our design to create new functional catalysts. Directly creating an original DOS for specific chemical application is difficult, therefore, we typically start from choosing an efficient catalyst as a template when we design DOS. Some experimental studies have proved the concept of the DOS engineering. $Pd_{0.5}Ru_{0.5}$ solid-solution alloy exhibits excellent NO_x reduction activity similar to or even exceeding that of Rh[9]. Ag–Rh alloy exhibits a hydrogen-storage property like Pd[10]. In addition, by alloying Pd with other metals, hydrogen-storage properties of Pd can be adjusted[13]. In the reaction of ethane formation, a metal catalyst can be replaced by transition metal carbides[14] because the reaction barriers with the catalysts of Pd and Rh are comparable to that of Ru–C and the barrier for Ru is comparable to that for Mo–C and Tc–C. Boron also is one option that can be used to adjust the number of d electrons to create a special DOS[15]. Although some progress in DOS engineering has been made, a scientific standard to evaluate the DOS shape between creation and the template is still lacking.

View Article Online
DOI: 10.1039/C9SC00912D

In this study, we investigated four binary alloys (Fe–W, Mo–Ru, Mn–Re, and Cr–Os) with solid-solution structures to explore the possibility of creating pseudo-Tc inspired by the concept proposed by Kitagawa[16]. All investigated elements are neighbors to Tc in the periodic table. Equal or similar compositions were adopted to ensure that the number of valence electrons in the alloys are the same or similar to Tc, which has been proven to be an important factor in breeding similar chemical properties[14,17,18]. By using density functional theory (DFT), the DOS was calculated to investigate the electronic structures. Excess energy and entropy were employed to discuss the stability and possibility of synthesis. Through this study, we propose some standards to evaluate the DOS shape difference.

2 Computational details

All the spin-polarized calculations were performed using the Vienna ab initio simulation package (VASP) [19,20] version 5.3.3, which is a plane-wave density functional code. The electron–electron exchange and correlation interactions were described by using the generalized gradient approximation (GGA) with the Perdew–Burke–Ernzerhof

View Article Online
DOI: 10.1039/C9SC00912D

(PBE)[21] functional form. The projector augmented-wave (PAW)[22,23] method was employed to describe the interaction between the core and valence electrons. The wave functions were expanded in a plane-wave basis set with a cutoff energy of 500 eV. The convergence criteria for energy was 1×10^{-5} eV/cell. Monkhorst-Pack[24] meshes of $9 \times 9 \times 9$ *k*-point sampling in the Brillouin zone were used for bulk models and $9 \times 9 \times 1$ were used for slab models. The tetrahedron method with Blöchl corrections[23] was employed to run an accurate total energy calculation. Both hcp and bcc phase of bulk structures were considered for these alloys because Mo, Fe, W, Cr, and Mn are bcc metal and Ru, Os and Re are hcp metal (the optimized models of bulk are shown in Fig. S1 and S2, as well as their XRD patterns calculated by VESTA). Here Mo–Ru alloy is taken as an example. For the slab models, we cleave (0001), and (100) surfaces for hcp and bcc metals because they are predominating growth surfaces. The vacuum layer was set about 15Å. The transition states were obtained by using the Climbing Image-Nudged Elastic Band method.[25]

3 Results and discussion

View Article Online
DOI: 10.1039/C9SC00912D

The chemical and physical properties of these alloys are determined by their electronic structures, which are typically represented as the DOS. The shape, intensity, band width, the contribution of s, p, d, and f orbitals of the DOS, and the valence and conduction levels are all the basic factors that breed the optical, magnetic, and thermodynamic properties[9]. To construct pseudo-Tc, an electronic structure analogous to that of Tc is required. Therefore, after optimization, we first calculated the DOS to evaluate the electronic structures of alloys. Fig. S3 shows the DOS of Mo-Ru alloys with different mixture ratios. The bcc-Mo_8Ru_8 and hcp-Mo_8Ru_8 have the same valance band width as Tc and their main DOS peaks located in the similar energy level as Tc, which indicates the similar electronic structure. However, for the other ratios, the large differences exist between alloys and Tc, which indicated the same valence electrons number is just one of important factors to create a similar electronic state. Furthermore, we also investigated the DOS of different kinds of alloys (Fe–W, Os–Cr, Mn–Re, and Mo–Ru alloys). The number of electrons in these alloys are the same as that of Tc. In Fig. S4, there are wide variations, which proved that the same orbital state is one important factor. For Mo-Ru alloys, the valence DOS was resulting from 4d-4d orbital

View Article Online
DOI: 10.1039/C9SC00912D

hybridization, while for other alloys, the natures of DOS came from 3d-5d orbitals hybridization.

Detailed analysis on hcp-Mo_8Ru_8, hcp-$Mo_{10}Ru_6$, and bcc-Mo_8Ru_8 have been carried out. We investigated the positions and intensities of specific peaks in the DOS, the band width, and the DOS area difference to evaluate the electronic structures. Some of the terms were already used to evaluate the electronic structures and properties[8,9]. Fig. 1(a) shows the total DOS of hcp-Tc_{16}, hcp-Mo_8Ru_8, hcp-$Mo_{10}Ru_6$, and bcc-Mo_8Ru_8. We separated the whole energy level into three parts with boundaries being marked as "canyons" (located at −2.31, −2.47, −2.16, and −2.42 eV for hcp-Tc_{16}, hcp-Mo_8Ru_8, hcp-$Mo_{10}Ru_6$, and bcc-Mo_8Ru_8, respectively) and the Fermi level. Fig. 1(b) demonstrates the shift of DOS peak positions among hcp-Mo_8Ru_8, bcc-Mo_8Ru_8, and hcp-$Mo_{10}Ru_6$, and hcp-Tc_{16}. In the low-energy-level range from negative infinity to the "canyon" boundary, three of the stronger DOS intensity areas can be easily identified (numbered as peaks 1, 2, and 3) in Fig. 1(a). All three alloys have similar peak positions corresponding to those of hcp-Tc_{16}. The peak position differences of hcp-Mo_8Ru_8, hcp-$Mo_{10}Ru_6$, and bcc-Mo_8Ru_8 from those of hcp-Tc_{16} are very small, with the largest

View Article Online
DOI: 10.1039/C9SC00912D

difference being 0.28 eV (for hcp-$Mo_{10}Ru_6$, as given in Table S1). The intensity differences between the identified peaks are also small and the largest difference is 0.20 states eV^{-1} $atom^{-1}$ (for hcp-Mo_8Ru_8, as given in Table S1). Here we only compare the position of the DOS peak center and the peak intensity because, according to these two terms, we can ascertain that the valance electrons are located at a similar energy level and can estimate how many electrons are at this energy level. In the middle part of the range from the "canyon" boundary to the Fermi level, a greater DOS difference between the Mo–Ru alloy and Tc can be observed. The electrons in orbitals near the Fermi level are more active, being sensitive to the environment, which leads to DOS shape changes. In the DOS of hcp-Tc_{16}, two single peaks and one split strong peak at −1.89, −1.17, and −0.56 eV can be clearly identified. However, in the alloy case, the DOS curves become more complex and it becomes difficult to differentiate the stronger intensity point from the others. For hcp-Mo_8Ru_8, the two split DOS peaks (−1.30 and −1.95 eV) correspond with the DOS peaks (at ca. −1.10 and −1.90 eV) in hcp-Tc_{16}. These is no DOS peak in hcp-Mo_8Ru_8 that can match the peak located at −0.56 eV in hcp-Tc_{16}, but some weak (noise-like) peaks are in this range. For hcp-$Mo_{10}Ru_6$, and bcc-

View Article Online
DOI: 10.1039/C9SC00912D

Mo_8Ru_8, from the "canyon" boundary to the Fermi level, the DOS shape is a broad platform. These DOS shape changes are caused by the formation of *n*-fold degenerate orbitals during alloying. Geometrically, for hcp-Tc_{16}, there are only Tc–Tc bonds, thus resulting in the same bond length and hybrid orbitals. For alloy systems, there are three kinds of bonds (Ru–Ru, Ru–Mo, and Mo–Mo), and the random arrangement of atoms leads to different bonds lengths. Electronically, for hcp-Tc_{16}, high symmetry means that the valence electrons are in the same electronic environment, so the electrons are localized in several specific energy levels, which leads to the stronger DOS peaks. For alloys systems, the lower symmetry and irregular electron distribution result in the broader DOS peaks. Therefore, according to this situation, we used a range of platform energy and the average intensity of the DOS to discuss their similarity. The energy range of the platform is signified in Fig. 1(a); the start and end positions were obtained from the local maximum DOS points and the values are listed in Table S2. The position differences of the platform and DOS intensities between alloys and hcp-Tc_{16} are less than 0.3 and 0.2 states eV^{-1} $atom^{-1}$, respectively. However, the choice of start and end

View Article Online
DOI: 10.1039/C9SC00912D

positions and the calculation of DOS intensity are not accurate enough because of the complex DOS shape.

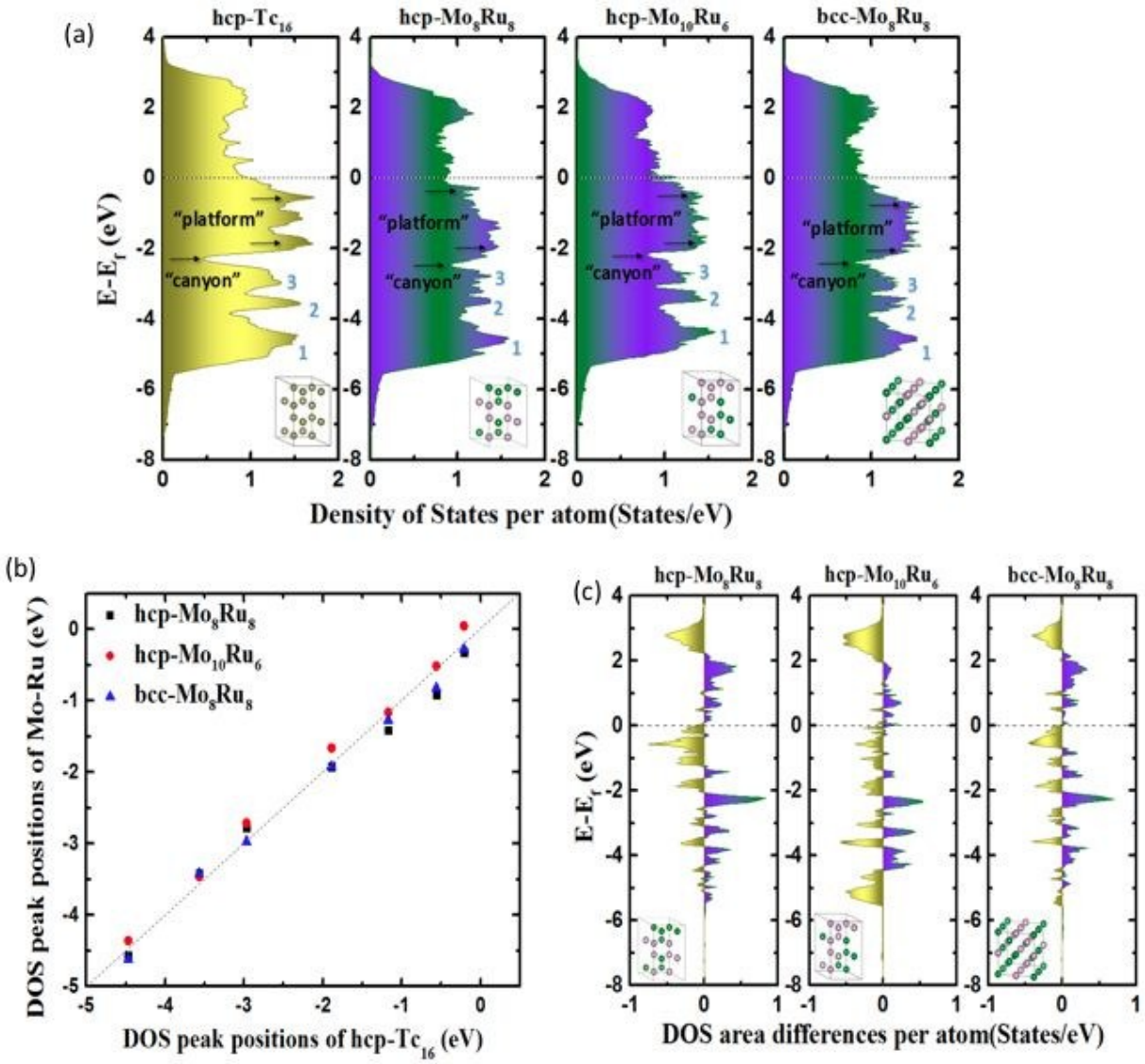

Fig. 1. (a) total DOS, (b) typical DOS peak positions, and (c) DOS integral differences of hcp-Mo_8Ru_8, hcp-$Mo_{10}Ru_6$, and bcc-Mo_8Ru_8 compared with that of hcp-Tc_{16}.

View Article Online
DOI: 10.1039/C9SC00912D

DOS area differences are represented by the DOS integral differences, and the integral of the differences was calculated by using the equation $\int_{-\infty}^{+\infty}|DOS_{Alloy} - DOS_{Tc}|d\varepsilon$. The DOS area differences between Mo–Ru alloy and Tc are shown in Fig. 1(c) and the different integral values (absolute values) are listed in Table 1. At the lower energy level from negative infinite to −2.3 eV (the largest positive integral differences), the area difference in hcp-$Mo_{10}Ru_6$ is much larger than those in hcp-$Mo_{10}Ru_6$ and bcc-Mo_8Ru_8. In the higher energy level range from −2.3 eV to the Fermi level, the area difference of hcp-$Mo_{10}Ru_6$ becomes smaller. In Fig. 1(c), for hcp-Mo_8Ru_8 near the Fermi level, the large difference area is caused by the platform. From the DOS of hcp-Tc_{16} in Fig. 1(a), we noticed a strong DOS peak (at −0.56 eV) near the Fermi level, while, for the alloys, it becomes weak. The integral differences in this local range follow the order of hcp-$Mo_{10}Ru_6$ < bcc-Mo_8Ru_8 < hcp-Mo_8Ru_8. hcp-$Mo_{10}Ru_6$ is the most promising candidate in the local range from −2.3 eV to the Fermi level. However, for whole energy level, a different conclusion is reached. Table 1 lists the values of DOS area differences; bcc-Mo_8Ru_8 has the smallest area differences with a value of 1.36

View Article Online
DOI: 10.1039/C9SC00912D

atom^{-1} for the whole energy level and the order is bcc-Mo_8Ru_8 < hcp-Mo_8Ru_8 (1.59 states eV^{-1} atom^{-1}) < hcp-$Mo_{10}Ru_6$ (1.63 states eV^{-1} atom^{-1}). These results agree with the conclusion that iso-valence electrons are one of the important factors in creating similar electronic structures. Finally, we compared the band widths of hcp-Mo_8Ru_8, hcp-$Mo_{10}Ru_6$, bcc-Mo_8Ru_8 and hcp-Tc_{16} listed in Table 1. For this term, the three alloys have a new order. hcp-Mo_8Ru_8 has almost the same d-band width as hcp-Tc_{16} (with a difference of 0.02 eV). The largest width difference is from bcc-Mo_8Ru_8 with a value of 0.48 eV. In addition, we also calculated the d-band center (listed in Table 1) as one factor for comparison. Based on the analysis above, all three alloys have the potential to act as pseudo-Tc, because each of them has respective similar features to those of Tc. bcc-Mo_8Ru_8 and hcp-Mo_8Ru_8 are evaluated as having more features that are similar to those of Tc, making them the first and second candidates to be pseudo-Tc.

Table 1. Integral differences per atoms, d-band width, and the d-band center.

View Article Online
DOI: 10.1039/C9SC00912D

	Integral differences	d-band width (eV)	Start (eV)	End (eV)	d-band center (eV)
hcp-Tc_{16}	0	11.58	−6.57	5.01	−1.33
hcp-Mo_8Ru_8	1.59	11.60	−7.02	4.58	−1.48
hcp-$Mo_{10}Ru_6$	1.63	11.15	−6.81	4.33	−1.44
bcc-Mo_8Ru_8	1.36	11.10	−6.82	4.28	−1.42

According to the electronic structure analysis above, hcp-Mo_8Ru_8 and bcc-Mo_8Ru_8 both have potential to be pseudo-Tc because of their highly similar DOS shapes. However, according to the phase diagram[26,27] of Mo–Ru alloy, at our suggested ratio, Mo–Ru alloy exists as phase-separated structures. A solid-solution structure is metastable. The excess energies[28] are calculated and displayed in Fig. 2(a) to evaluate the phase stability and possibility for synthesis. The calculated excess energies exhibit the same tendency as seen in the phase diagram[26,27] and as noted in other reports[29]. It is obvious that the hcp type is the most stable phase when the Ru ratio is >60% because, in this Ru ratio range, negative excess energy is reported in this study and it is experimentally proved[27]. The bcc types of Mo–Ru alloys are unstable in the whole Ru ratio range because of positive excess energy. In Fig. 2(a), we also noticed that bcc-

View Article Online
DOI: 10.1039/C9SC00912D

$Mo_{14}Ru_2$ and hcp-$Mo_{14}Ru_2$, bcc-Mo_8Ru_8 and hcp-Mo_8Ru_8 have very similar excess energies. By comparing their XRD patterns shown in Fig. S1 and S2, we found that after optimization, hcp-$Mo_{14}Ru_2$ transformed to bcc type, and bcc-Mo_8Ru_8 transformed to hcp type, which indicated with solid-solution structures, Mo-Ru alloy in those ratios had only one stable phase. For Mo-Ru alloy with high Ru ratio such as Mo_6Ru_{10}, Mo_4Ru_{12}, and Mo_2Ru_{14}, their excess energies split, the XRD patterns suggested bcc-Mo_6Ru_{10}, bcc-Mo_4Ru_{12}, and bcc-Mo_2Ru_{14} had transferred into fcc phase, while hcp-Mo_6Ru_{10}, hcp-Mo_4Ru_{12}, and hcp-Mo_2Ru_{14} kept hcp phase. The existence of both hcp and fcc phase for Ru applies a good explanation for this result. The fcc phase of Ru as the stable structure for Ru in nanoparticle had been discovered and synthesized[30]. The stability of its alloy in fcc phase also been evaluated in experimental[31] and theoretical[32]. The phase of Mo-Ru alloy with high Ru ratio transfers from bcc to fcc instead of hcp because of the similarity of electronic structure between bcc and fcc phase. For bcc and fcc phase, the t_{2g}, and e_g orbitals are separate, d_{xy}, d_{yz}, and d_{xz} orbitals highly hybridize, which performed as the totally same DOS shape in crystal, the same results for the orbitals of d_{x2-y2} and d_{z2}. However for the hcp phase, the t_{2g} orbitals were separated, the orbitals of d_{xz} and d_{yz} locate on the same energy level, and the orbitals of d_{xy} and d_{x2-y2} locate on the same energy level, while the orbitals d_{z2} locates on the different energy level. In our suggested alloy range, neither the hcp phase (hcp-Mo_8Ru_8)

View Article Online
DOI: 10.1039/C9SC00912D

nor the bcc phase (bcc-Mo_8Ru_8) is stable because of the positive excess energy. They are thermodynamically unstable. However, the excess energies are very small, with values of 0.052 and 0.059 eV/atom for hcp-Mo_8Ru_8 and bcc-Mo_8Ru_8, respectively.

The effect of entropy on excess energy[33] was considered to discuss the relative stabilities of hcp-Mo_8Ru_8 and bcc-Mo_8Ru_8 at finite temperature. The entropy here includes configurational and vibrational entropies. In our random solid-solution models, we fully considered the effect of symmetry in the bulk system to reduce the possible configurations in hcp and bcc phases. The configurational entropy reaches a maximum of 5.97×10^{-5} eV/K per atom, which is similar to the published data for binary alloys[33,34]. For the phase-separated structure, the number of possible structures is unity. The effect of vibrational entropy (Table S3) is very small compared with the configurational entropy (5.97×10^{-5} eV/K per atom) after subtracting the part from the phase-separated structure. Even when the temperature reaches 1000 K, the thermodynamic effect from vibrational entropy is 7.28×10^{-6} eV/K per atom for hcp-Mo_8Ru_8, while it is 1.96×10^{-5} eV/K per atom for bcc-Mo_8Ru_8. That is, increasing configurational entropy is one of most efficient methods for creating a phase-stable alloy.

View Article Online
DOI: 10.1039/C9SC00912D

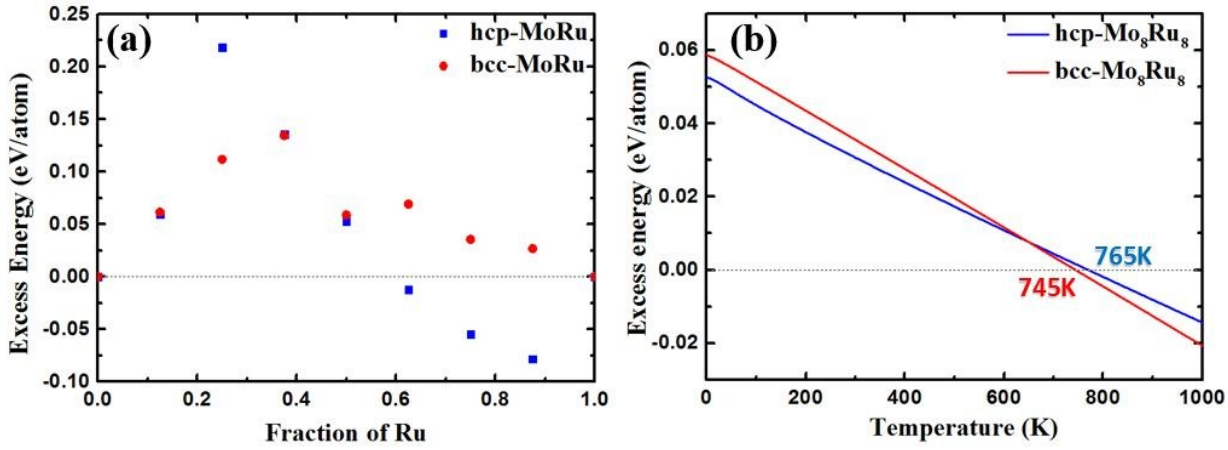

Fig. 2. Excess energy of Mo – Ru alloy with both hcp and bcc phase (a) excess energy and (b) excess energy after entropy correction.

Fig. 2(b) shows the excess energy after entropy correction. In the temperature range from 0 to 765 K for hcp-Mo_8Ru_8 and to 745 K for bcc-Mo_8Ru_8, the Mo–Ru alloys are still unstable because of positive values. However, the excess energies keep deceasing as the temperature increases. When the temperatures are up to 765 K for hcp-Mo_8Ru_8 and up to 745 K for bcc-Mo_8Ru_8, solid-solution Mo–Ru alloys can be stable and synthesized. Furthermore, depending on the synthesis conditions, hcp and bcc can be retained up to a certain range of temperature[35]. That is, when hcp-Mo_8Ru_8 and bcc-Mo_8Ru_8 are formed by cooling, they may be stable in a lower temperature range[34]. These excess energy

View Article Online
DOI: 10.1039/C9SC00912D

results suggest that solid-solution Mo_8Ru_8 for both bcc and hcp types can be synthesized and stable when the temperatures are up to 745 and 765 K, respectively. When combined in the form of nanoparticles, Mo–Ru can be expected to be synthesized at a lower temperature because of its large specific surface area, which gives the surface energy a larger weight in the total energy system of the alloy[36–37].

The basic idea for catalyst design in our study is that the catalytic activities fundamentally originate from the electronic structures presented as DOS, creating a similar electronic structures (DOS) means the similar catalytic process in chemistry. In order to validate our idea, we simulated the surface reactions of CO oxidation and N_2 dissociation for NH_3 synthesis over monometals (Tc, Mo, Ru) and Mo-Ru alloys. Up to now these is no study of Tc in catalytic applications, while plenty of studies for neighbor metals (Ru and Mo) can be found[38-43]. From those studies, we can find some insights as follows. Ru (Ru-Cu[38], Ru-Pt[39], Ru-O[40] for CO oxidation and Ru-Ba[41] for NH_3 synthesis) and Mo ($Rh/SiO_2/Mo$[42] for CO and Mo cluster[43] for N_2 dissociation) related catalysts perform good activity toward CO oxidation and NH_3 synthesis. However, neither monometal Ru nor Mo is the efficient catalyst to run those reactions. Slight

View Article Online
DOI: 10.1039/C9SC00912D

modifications may lead to enhance their catalytic activity. On the other hand, comparing the nature of Mo and Ru in NH_3 synthesis, Tc may locate in hot-spots area of steady-state TOF[44] according to the position of Tc in periodic table. For hcp-Mo_8Ru_8, we constructed four slab models as shown in Fig. S5 to investigate all the possible sites in hcp-Mo_8Ru_8 considered. Here we did not cleave the surface based on bcc-Mo_8Ru_8, because according to the stability analysis above, bcc-Mo_8Ru_8 had transformed to hcp phase (Fig. S1). In order to make sure that our approach also works for the partial density of states and local density of states, we evaluated the DOS shape similarity of alloy surface to that of Tc(0001), as well as the DOS of local active sites. Figs. S6 and S7 show the DOS area differences, and Table 2 lists the values of d-band center and DOS area integral differences. After alloying, the d-band centers of four MoRu(0001) surface models were -1.70 eV, -1.32 eV, -1.29 eV, and -1.47 eV, which are close to -1.40 eV of Tc surface, and different from those of Ru(0001) (-1.90 eV) and Mo(100) (-0.99 eV), except for MoRu(0001)-1, which is a Ru-segregated surface model. The active sites on Mo-Ru alloy show more similar electronic structure with the d-band center values of -1.39 eV, -1.38eV, -1.39eV for MoRu(0001)-2, MoRu(0001)-3, and

View Article Online
DOI: 10.1039/C9SC00912D

MoRu(0001)-4, respectively. The DOS area differences obtained for those three surfaces were confirmed to be small from Figs. S6, S7 and Table 2. Both of d-band center and DOS area different suggest that the local electronic state of Tc had been reproduced by alloying Mo-Ru. Next, we simulated the catalytic reactions on the surfaces.

Table 2 The d-band center and the DOS integral differences of surface (S) and active site (AS) for each model. The active site for Mo(100) is hcp site of Mo_4; The active sites for Tc(0001), Ru(0001), MoRu(0001)-1 are fcc/hcp site of Tc_3, Ru_3, and Ru_3; The active sites for MoRu(0001)-2, MoRu(0001)-3, and MoRu(0001)-4 are fcc/hcp sites of Mo_2Ru.

S/AS	d-band center (eV)	Integral differences
Tc(0001) S(AS)	-1.40	0
Ru(0001) S(AS)	-1.90	5.49
Mo(100) S(AS)	-0.99	4.75
MoRu(0001)-1 S(AS)	-1.70	3.06
MoRu(0001)-2 S	-1.32	2.99
MoRu(0001)-2 AS	-1.39	2.83
MoRu(0001)-3 S	-1.29	2.45
MoRu(0001)-3 AS	-1.38	2.38
MoRu(0001)-4 S	-1.47	2.99
MoRu(0001)-4 AS	-1.39	2.99

View Article Online
DOI: 10.1039/C9SC00912D

The CO oxidation on catalyst surface usually is accompanied by adsorption as the initial process. The fcc, top and 4 fold-hollow sites are the most stable sites for CO adsorption on Tc(0001), Ru(0001), Mo(100) with the values of -1.80eV, -1.91eV, -2.21eV shown in Table S4 (Adsorption structures are also shown in Table S4), respectively. However, the adsorption structure of CO on top sites is crucially important for oxidation[45-46]. On Tc(0001) surface, The calculated CO adsorption energy on top sites is the highest (-1.72eV compared to -1.91eV, -1.73eV on top site of Ru(0001), Mo(100), respectively). Table S5 summarizes the adsorption structures and energies of CO on four MoRu(0001) surfaces. The adsorption energies for CO on MoRu(0001) perform bipolar distribution between Ru-top site (-1.95 to -2.08eV) and Mo-top site (-1.59 to -1.73eV). After alloying, more electrons distribute on Ru potentially enhancing the electron back-donation capability, which will lead to the stronger CO adsorption. Contrary to CO adsorption, O is more favorable on the Mo-related sites. The most stable site is Mo_3-3fold hollow sites (less than -4.00eV as shown in Table S6). The $MoRu_2$-3fold hollow sites have the most similar adsorption energies to that of Tc (-

View Article Online
DOI: 10.1039/C9SC00912D

3.43eV and -3.01eV of $MoRu_2$-hcp and $MoRu_2$-fcc on MoRu(0001)-4 compared to the -3.67eV and -3.01eV of Tc_3-hcp and Tc_3-fcc shown in Table S4).

The catalytic processes of CO oxidation over Tc(0001), Ru(0001), Mo(100), and MoRu(0001) are summarized in Fig. 3 (Initial states (IS), Transition states (TS), and Final states (FS) are shown in Fig. S8). The analysis for adsorption structures above suggests that the molecular CO is favorable on Ru-top site while the atomic O is favorable on Mo_3-3fold-hollow site. The MoRu(0001) has both kinds of adsorption sites, and these sites reduce the competitive adsorption by separately adsorbing molecular CO and atomic O, causing the most stable co-adsorption (shown in Table 3). This indicates that CO oxidation will follow the Langmuir-Hinshelwood (LH) model on MoRu(0001). In order to investigate the processes of different electronic structures driving reaction, LH model was employed for CO oxidation on all the surface models. The calculated activation energy of $CO_{(ad)} + O_{(ad)} \rightarrow CO_{2(ad)}$ on Tc(0001) is 1.73 eV, higher than that of Ru(0001) and Mo(100) with the values of 1.51 eV and 0.99 eV. For Mo(100), it executes the different reaction process due to the totally different morphology. For Ru(0001), lower activation energy is due to the weak O adsorption

View Article Online
DOI: 10.1039/C9SC00912D

energy (-2.90 eV compared with -3.67eV on Tc(0001)). For the MoRu(0001) surfaces, they have activation energies with the values of 1.80eV, 1.64eV, 1.64eV, 2.20eV for the four slab models, respectively, as shown in Table 3. The activation energies distribute around the value of Tc, i.e. 1.73eV, which we can conclude that Mo-Ru will show the catalytic properties similar to that of Tc. Those energy deviation on MoRu(0001) were due to the randomness of solid-solution structures. Unlike monometal, there are many different catalytic sites for CO oxidation, which extend the energy range with a certain average value similar to Tc. These results also confirmed DOS analysis that the moderate DOS shape of MoRu alloy comparing with that of hcp-Tc_{16}. It should be noticed that Mo is calculated as the best catalyst for CO oxidation because of lowest activation energy (0.99 eV) by assuming the same LH mechanism just for a simple comparison of different catalysts. However, much stronger O adsorption (-4.08 eV) than CO (-2.21eV) on the same hollow sites of Mo(100) will make Mo surface oxidized, instead of co-adsorption structure, which will lead to different mechanism such as Eley-Rideal mechanism. This will make Mo be a poor catalyst for CO oxidation in actual experiment.

View Article Online
DOI: 10.1039/C9SC00912D

Table 3 Activation energy (E_a), reaction energy (E_r) of CO oxidation, and co-adsorption energy ($E_{Co\text{-}ads}$) of molecular CO and atomic O on these surfaces ($E_{Co-ads} = E_{total} - E_{slab} - E_{CO} - \frac{1}{2}E_{O_2}$)

Surface	E_a (eV)	E_r (eV)	E_{Co-ads} (eV)
Tc(0001)	1.73	1.57	-5.22
Ru(0001)	1.51	1.39	-4.73
Mo(100)	0.99	-0.02	-4.97
MoRu(0001)-1	1.80	1.34	-4.68
MoRu(0001)-2	1.63	1.54	-5.91
MoRu(0001)-3	1.63	1.60	-5.86
MoRu(0001)-4	2.20	2.00	-5.92

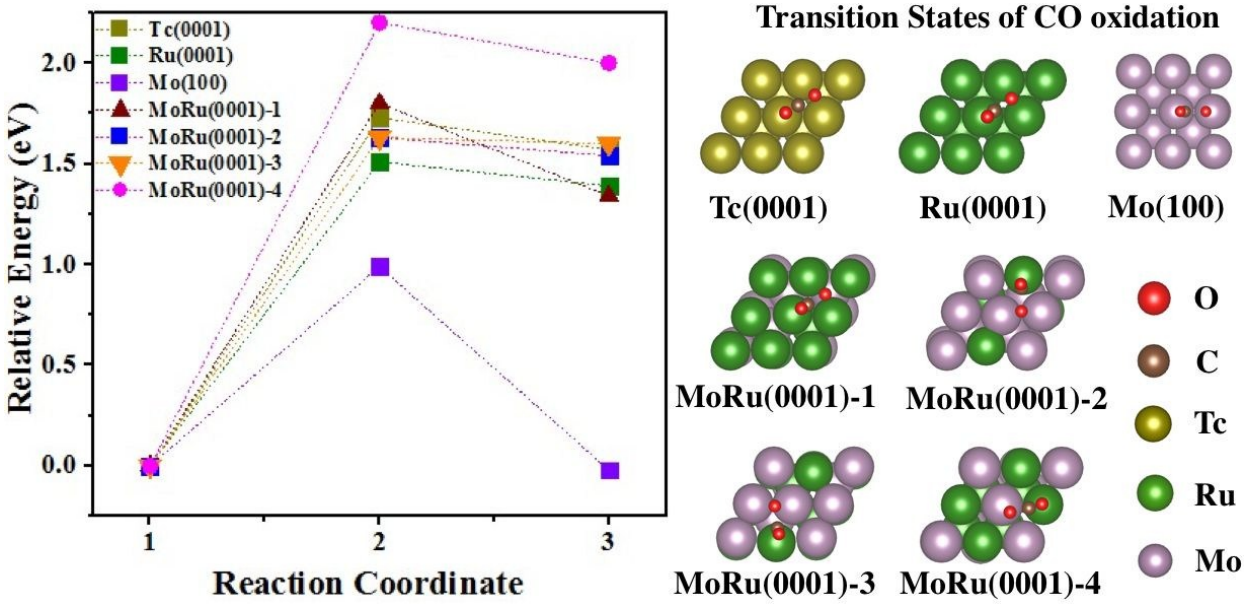

View Article Online
DOI: 10.1039/C9SC00912D

Fig. 3 The energy pathway for CO oxidation process (CO* + O* $\rightarrow$ CO_2*) on Tc(0001), Ru(0001), Mo(100), and four MoRu(0001) surfaces. The calculated energy pathway of CO oxidation and the structures of TS for CO oxidations. The IS, TS, and FS structures are shown in Fig. S8.

We next investigated the catalytic activity for NH_3 synthesis. In NH_3 synthesis process, amount of the experimental and theoretical works had clarified the N_2 dissociation as the rate-determining step[47-48]. Furthermore, it is reported that too weak N_2 adsorption energies and too strong binding of intermediate (such as *N) also will prevent the reaction process[44, 49]. Therefore, the best catalyst will have an ideal balance between activation energy (E_a) and adsorption energy of *N and N_2 (evaluated by reaction energy (E_r)), which locates in a suitable area described by Bell-Evans-Polanyi or Brønsted-Evans-Polanyi scaling relationship. In Aayush's study[44], Mo and Ru have the catalytic activities beside suitable area, which are suffering the too stronger N adsorption interaction (Mo metal), and higher N_2 dissociation activation energy (Ru metal), respectively. Because Tc is located between Mo and Ru in the periodic table, it

View Article Online
DOI: 10.1039/C9SC00912D

is expected being an excellent catalyst for NH_3 synthesis, as well as our designed pseudo-Tc materials (Mo-Ru alloy). As shown in Table S7, N_2 adsorbed at bridge sites and the adsorption energies are -0.91eV -0.32 eV, 0.07eV on Mo(100), Tc(0001), Ru(0001), respectively. Also for N_2 on MoRu(0001), the bridge site is a favorable site as shown in Table S7. The adsorption energies distribute in the range from -0.36eV to -0.89eV, which is due to non-uniform adsorption sites of MoRu(0001) surface. The energy profile of N_2 dissociation on those surfaces were shown in Fig. 4, the corresponding key properties including the activation energy, reaction energy are summarized in Table 4. As reported results[44], the Mo have the lower N_2 activation energy (0.67eV) and reaction energy (-3.20eV), suffering from a strong *N binding energy. The activation energy is as large as 1.53eV, indicating the N_2 is not easily dissociated at room temperature. The activation energy on Tc is 1.28eV while the reaction energy is -1.53eV, which is close to the suitable area of steady-state TOF in NH_3 synthesis. Just following our design, Mo-Ru alloy exhibits similar catalytic activity as Tc in N_2 dissociation. From Table 4, on the MoRu(0001) surface, the activation energies for N_2 dissociation concentrate in narrow range (1.23eV to 1.36eV), close to

View Article Online
DOI: 10.1039/C9SC00912D

1.28eV of that on Tc(0001). The structures of TS shown in Fig. 4 on MoRu(0001) are similar to Tc (one N atom is on the top-site and the other N is on the bridge-site of opposite direction). The elongated N-N distances in TS structure on Mo-Ru surfaces are 1.89 Å, 1.90 Å, 1.90Å, which are close to N-N distances of 1.91Å on Tc(0001). This indicates the process of N_2 dissociation on Mo-Ru is similar to that of on Tc(0001), $Mo_{0.5}$-$Ru_{0.5}$ alloy reproduced the chemical properties of Tc as our design. Also, we noticed one exception of MoRu(0001)-1(Ru-skin), N_2 dissociation on this surface suffer the highest activation energy with the value of 3.43eV. This is because the reaction proceeds in different way. In Table S7 of MoRu(0001)-1, N_2 adsorbed on top sites with end-on configuration while tilted end-on or side-on adsorptions are observed in other surfaces. Before forming the most stable N-hollow adsorption structures, two dissociated N atoms must be first formed from the straight end-on configuration, which leads to the higher reaction energy (3.18eV). MoRu(0001)-1 is understood as an extreme example of core-shell and phase-separated structures in alloy catalyst structures.

View Article Online
DOI: 10.1039/C9SC00912D

Table 4 The activation energy(E_a), reaction energy (E_r) for N_2 dissociation, and adsorption energy ($E_{ads\text{-}N2}$) of molecular N_2 ($E_{ads-N2} = E_{total} - E_{slab} - E_{N_2}$), here listed E_{ads-N2}were calculated by using IS.

Surface	E_a (eV)	E_r (eV)	E_{ads-N2} (eV)
Tc(0001)	1.28	-1.52	-0.32
Ru(0001)	1.54	-0.41	0.07
Mo(100)	0.67	-3.20	-0.91
MoRu(0001)-1	3.43	3.18	-0.49
MoRu(0001)-2	1.28	-2.10	-0.62
MoRu(0001)-3	1.23	-2.19	-0.69
MoRu(0001)-4	1.36	-1.59	-0.39

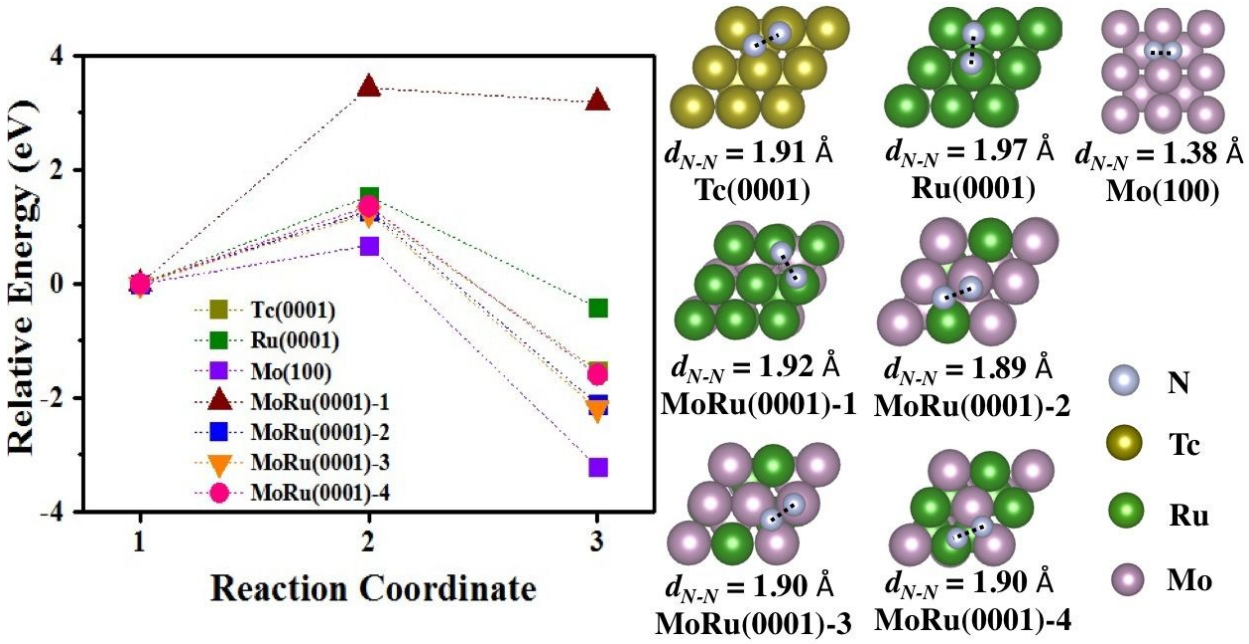

View Article Online
DOI: 10.1039/C9SC00912D

Fig. 4 The energy pathway for the N_2 dissociation process ($N_2^* \rightarrow 2N^*$) on Tc(0001), Ru(0001), Mo(100), and four MoRu(0001) surfaces. The calculated energy pathway of N_2 dissociation and the structures of TS for N_2 dissociation. The IS, TS, and FS are shown in Fig. S9.

4 Conclusions

In summary, we theoretically designed a new pseudo-Tc material of Mo–Ru alloy and investigated its electronic structure and phase stability. From the DOS analysis, hcp-$Mo_{10}Ru_6$, hcp-Mo_8Ru_8, and bcc-Mo_8Ru_8 were identified as suitable candidates of pseudo-Tc because they have DOS shape and peak distributions similar to Tc throughout the whole energy level. The DOS area differences from that of Tc follow the order of bcc-Mo_8Ru_8 < hcp-Mo_8Ru_8 < hcp-$Mo_{10}Ru_6$. In the suggested Ru ratio range, neither hcp-Mo_8Ru_8 nor bcc-Mo_8Ru_8 is stable because of the positive excess energy; however, the values are small (0.052 eV/atom for hcp-Mo_8Ru_8 and 0.059 eV/atom for bcc-Mo_8Ru_8). The effect of entropy was investigated to evaluate the stability at finite temperature, especially configurational entropy. After entropy correction, hcp-Mo_8Ru_8

View Article Online
DOI: 10.1039/C9SC00912D

and bcc-Mo_8Ru_8 are stable when the temperature is up to 765 and 745 K, respectively. This result agrees well with the preceding study for bulk Mo–Ru[25]. However, the excess energy and high-temperature range also evidenced the limitations of using the bulk form in synthesis, while using nanoparticles may be a breakthrough for synthesizing Mo–Ru alloy in the low-temperature range because of the larger contribution of the surface energy to the energy of the whole system. In reaction simulation of CO oxidation and N_2 dissociation, MoRu(0001) has the related energies (adsorption energy, activation energy, reaction energy), reaction process and related structures (IS, TS, and FS) similar to that of Tc(0001). The results indicate our designed solid-solution $Mo_{0.5}Ru_{0.5}$ alloy can reproduce the chemical properties of Tc. The existence of exceptions (RuMo(0001)-1, Ru-skin) proved the importance of local site structure, it revealed the limitation of Core-shell and phase-separated structures in catalysts design. Our results on electronic structure and phase stability have important implications in materials design for catalysts, particularly for binary alloys.

Conflicts of interest

View Article Online
DOI: 10.1039/C9SC00912D

There are no conflicts to declare.

Acknowledgements

Activities at the INAMORI Frontier Research Center are supported by KYOCERA Corporation. This work was supported by JST-ACCEL Grant No. JPMJAC1501, Japan. Prof. Takayoshi Ishimoto (Hiroshima University, Hiroshima, Japan) is acknowledged for the numerous discussions and helpful comments during this work.

Notes and references

(1) C. Perrier and E. Segré, *Nature*, 1947, **159**, 24.

(2) F. N. Skomurski and K. M. Rosso, *Environ. Sci. Technol.*, 2010, **44**, 5855–5861.

(3) C. D. Taylor, *J. Phys. Chem. C*, 2014, **118**, 10017–10023.

(4) C. D. Taylor, *J. Nucl. Mater.,* 2011, **408**, 183–187.

(5) C. D. Taylor, *J. Metall.*, 2011, 954170.

(6) D. D. Keiser, D. P. Abraham and J. W. Richardson, *J. Nucl. Mater.,* 2000, **277**, 333–338.

View Article Online
DOI: 10.1039/C9SC00912D

(7) G. N. Pirogova, N. M. Prokhorets, T. A. Lagutina and R. I. Korosteleva, *Phys. Chem.,* 1982, **31**, 747–751.

(8) H. Kobayashi, K. Kusada and H. Kitagawa, *Acc. Chem. Res.*, 2015, **48**, 1551–1559.

(9) K. Sato, H. Tomonaga, T. Yamamoto, S. Matsumura, N. D. B. Zulkifli, T. Ishimoto, M. Koyama, K. Kusada, H. Kobayashi, H. Kitagawa and K. Nagaoka, *Sci. Rep.*, 2016, **6**, 28265.

(10) A. Yang, O. Sakata, K. Kusada, T. Yayama, H. Yoshikawa, T. Ishimoto, M. Koyama, H. Kobayashi and H. Kitagawa, *Appl. Phys. Lett.*, 2014, **105**, 153109.

(11) J. Greeley, J. K. Nørskov, L. A. Kibler, A. M. El-Aziz and D. M. Kolb, *ChemPhysChem*, 2006, 7, 1032−1035.

(12) J. K. Nørskov, T. Bligaard, J. Rossmeisl and C. H. Christensen, *Nat. Chem.*, 2009, **1**, 37−46.

(13) T. Yayama, T. Ishimoto and M. Koyama, *J. Alloys Compd.*, 2015, **653**, 444.

(14) S. Sahoo, A. C. Reber and S. N. Khanna, *J. Phys. Chem. A*, 2015, **119**, 12855−12861.

View Article Online
DOI: 10.1039/C9SC00912D

(15) K. Kobayashi, H. Kobayashi, M. Maesato, M. Hayashi, T. Yamamoto, S. Yoshioka, S. Matsumura, T. Sugiyama, S. Kawaguchi, Y. Kubota, H. Nakanishi and H. Kitagawa, *Angew. Chem., Int. Ed.*, 2017, **56**, 6578–6582.

(16) Personal communication with Prof. Hiroshi Kitagawa of Kyoto University within ACCEL project, Japan Science and Technology Agency (https://www.jst.go.jp/kisoken/accel/en/research_project/ongoing/h27_01.html).

(17) R. B. Levy and M. Boudart, *Science*, 1973, **181**, 547−549.

(18) N. Ji, T. Zhang, M. Zheng, A. Wang, H. Wang, X. Wang and J. Chen, *Angew. Chem., Int. Ed.*, 2008, **47**, 8510−8513.

(19) G. Kresse and J. Furthmüller, *Phys. Rev. B*, 1996, **54**, 11169–11186.

(20) G. Kresse and J. Hafner, *Phys. Rev. B*, 1993, **47**, 558–561.

(21) J. P. Perdew, K. Burke and M. Ernzerhof, *Phys. Rev. Lett.*, 1996, **77**, 3865–3868.

(22) G. Kresse and J. Joubert, *Phys. Rev. B*, 1999, **59**, 1758–1775.

(23) P. E. Blöchl, *Phys. Rev. B*, 1994, **50**, 17953–17979.

(24) H. J. Monkhorst and J. D. Pack, *Phys. Rev. B*, 1976, **13**, 5188–5192.

(25) G. Henkelman, B. P. Uberuaga and H. A. Jónsson, *J. Chem. Phys.*, 2000, **113**, 9901-9904.

View Article Online
DOI: 10.1039/C9SC00912D

(26)T. B. Massalski, H. Okamoto and P. R. Subramanian, Binary Alloy Phase Diagrams, ASM International, Materials Park, Ohio, USA, 1990.

(27)B. Predel, O. Madelung, Li-Mg–Nd-Zr. Springer, Berlin, Heidelberg, 1997.

(28)R. Ferrando, A. Fortunelli and G. Rossi, *Phys. Rev. B*, 2005, **72**, 085449.

(29)S. H. Kessler, D. G. Abrecht, R. A. Clark and J. M. Schwantes, *J. Alloys Compd.*, 2016, **689**, 969–976.

(30)K. Kusada, H. Kobayashi, T. Yamamoto, S. Matsumura, N. Sumi, K. Sato, K. Nagaoka, Y. Kubota and H. Kitakawa, *J. Am. Chem. Soc.*, 2013, **135**, 5493–5496.

(31)B. Huang, H. Kobayashi, T. Yamamoto, S. Matsumura, Y. Nishida, K. Sato, K. Nagaoka, S. Kawaguchi, Y. Kubota and H. Kitagawa, *J. Am. Chem. Soc.*, 2017, **139**, 4643–4646.

(32)Y. Nanba, T. Ishimoto, and M. Koyama, *J. Phys. Chem. C.*, 2017, **121**, 49, 27445-27452

(33)T. Ishimoto, and M. Koyama, *J. Phys. Chem. Lett.*, 2016, **7**, 736–740.

(34)H. B. Liu, U. Pal, R. Perez, and J. A. Ascencio, *J. Phys. Chem B*, 2006, **110**, 5191–5195.

(35)N. Toshima, *Pure Appl. Chem.*, 2000, **72**, 317–325.

View Article Online
DOI: 10.1039/C9SC00912D

(36) R. Kubo, *J. Phys. Soc. Jpn.*, 1962, **17**, 975–986.

(37) G. Schmid, Clusters and Colloids. From Theory to Applications. VCH, Weinheim, 1994.

(38) H. Kobayashi, M. Yamauchi, H. Kitagawa, Y. Kubota, K. Kato and M. Takata, *J. Am. Chem. Soc.*, 2010, **132**, 5576–5577.

(39) M. Yu and E. B. Yeager, *J. Electroanal. Chem.*, 1998, **441(1–2)**, 77-81.

(40) A. Böttcher, H. Niehus, S. Schwegmann, H. Over and G. Ertl, *J. Phys. Chem. B*, 1997, **101**, 11185-11191.

(41) C. H. Liang, Z. B. Wei, Q. Xin and C. Li, *React. Kinet. Cat. Lett.*, 2004, **83**, 39-45.

(42) S. M. Mcclure, M. Lundwall, F. Yang, Z. Zhou and D. W. Goodman, *J. Phys. Chem. C,* 2009, **113**, 9688-9697.

(43) A. Bérces, S. A. Mitchell and M. Z. Zgierski, *J. Phys. Chem. A*, 1998, **102**, 6340-6347.

(44) A. R. Singh, J. H. Montoya, B. A. Rohr, C. Tsai, A. Vojvodic, and J. K. Norskov, *ACS Catal.*, 2018, **8**, 4017-4024.

(45) J. L. C. Fajin, M. N. D. S. Cordeiro and J. R. B Gomes, *J. Phys. Chem. C*, 2008, **112**, 17921-17302.

View Article Online
DOI: 10.1039/C9SC00912D

(46)B. T. Qiao, X. F. Wang, X. F. Yang, L. F. Allard, Z. Jiang, Y. T. Cui, J. Y. Liu, J. Li and T. Zhang, *NATU. CHEM.*, 2011, **3**, 634-641

(47)K. Honkala, A. Hellman, I. Remediakis, A. Logadottir, A. Carlsson, S. Dahl, C. H. Chris- tensen and J. K. Nørskov, *Science*, 2005, **307**, 555–558.

(48)G. Ertl, *Catal. Rev.*, 2006, **21**, 201–223.

(49)A. Vojvodic, A. J. Medford, F. Studt, F. Abild-Pedersen, T. S. Khan, T. Bligaard and J. K. Nørskov, *Chem. Phys. Lett.*, 2014, **598**, 108–112.

View Article Online
DOI: 10.1039/C9SC00912D